Polarization conversion-based molecular sensing using anisotropic plasmonic metasurfaces

R. Verre,[1,] N. Maccaferri,[2] K. Fleischer,[3] M. Svedendahl,[1] N. Odebo Länk,[1] A. Dmitriev,[1] P. Vavassori,[2,4] I.V.Shvets[3] and M. Käll[1]*

[1]*Department of Physics, Chalmers University of Technology,* 412 96 *Göteborg, Sweden*

[2]*CIC nanoGUNE, 20018 San-Sebastian, Spain*

[3]*Trinity College Dublin and Center for Research on Adaptive Nanostructures and Nanodevices (CRANN), Dublin, Ireland*

[4] IKERBASQUE, Basque Foundation for Science, 48013 Bilbao, Spain

***E-mail: ruggero.verre@chalmers.se**

Supporting Information

Table of Contents

1) Materials and Methods
    a. Sample fabrication
    b. Optical characterization
    c. Surface functionalization
2) Analytical calculations
    a. Derivation of Equation (1)
    b. Transfer matrix approach
3) Additional results
    a. Simulated extinction using FDTD
    b. Tunability of the rotation angle
    c. Bulk refractometric sensing
    d. Relation between rotation and refractive index sensitivity
    e. Alternative setup for measuring the rotation angle

1) Materials and Methods

a. Sample fabrication

The samples were produced using the hole-mask colloidal lithography technique. First, the glass substrates were cleaned in acetone and IPA and sonicated. PMMA A4 was spun on the sample at 3000 rpm and annealed in an oven furnace at 180°C for 10 minutes. A quick oxygen plasma treatment (50 W for 5 s) rendered the surface hydrophilic and a PDDA-water solution (0.2%) was dispersed on the samples for 30 s and then rinsed in deionized water for 10s to induce positive charges on the surface. Polystyrene beads (100nm in diameter, 0.01% diluted in deionized water) were subsequently dispersed for 45s on the substrate by dropcasting, and successively rinsed for 30 seconds in running water. A 10 nm Au mask was deposited on the sample and the latex beads removed by tape stripping. The resulting Au mask was then used as a deposition mask. The PMMA was first etched by O_2 plasma, at 50 W at 250 mTorr for 5 minutes to allow a large enough undercut for the dimer deposition. A 1nm Cr adhesion layer was first deposited at both positive and negative angles of incidence of 13.5°. Afterwards, Au dimers of a total thickness of 40nm each were deposited by evaporating at both positive and negative angles of incidence of 13.5° and lift-off in acetone was performed. As the deposition would also induce a shrinking of the mask due to side deposition, positive and negative deposition were alternated every 5nm. All samples were annealed at 250°C for 10 minutes prior to characterization.

b. Optical characterization

The extinction data were collected using a Cary 3000 spectrophotometer. The rotation and the ellipticity were measured using a home-made setup. Light from a Xe lamp passes through a Rochon polarizer and, after the transmission through the sample, passes through a photoelastic modulator (Hinds Instruments, USA), an analyzer polarizer and a monochromator (TMC300, Bentham, UK) before finally reaching a Si diode detector. For micro-measurements, a long working distance 100X microscope objective was inserted in the light path before the sample. The transmitted light was collimated through a lens system and light was then focused once again into the monochromator. An aperture was used to reduce the imaged region. For the reflection measurements a different setup was used. A white-light laser and an acousto-optic modulator (Fianium, UK) were used as a monochromatic light source and the samples were illuminated with linearly polarized light. After reflection on the sample, a beam splitter directed the light towards the photoelastic modulator and a polarizer before hitting a photodiode.

c. Surface functionalization

Prior to the sensing experiments, the samples were cleaned in a basic piranha solution (HNO_3: H_2O:H_2O in a ratio of 6:1:1) at 80°C for 10minutes and rinsed in deionized water before loading into a flow cell. Biotinylated bovin serum albumin (bBSA, Sigma Aldrich), with a concentration of 100ug/mL was diluted in a phosphate buffer solution (~0.01 mol/L), was first adsorbed on the surface. After rinsing, neutravidin, also diluted in phosphate buffer, was injected in the flow cell.

2) Analytical calculations

a. Derivation of Equation (1)

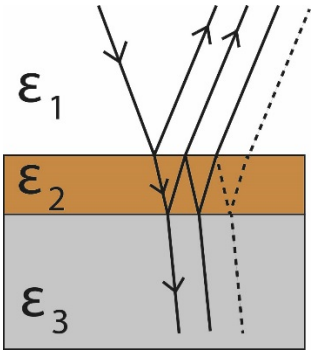

Figure S1. Sketch of the 3 layers model used for the derivation of Equation 1 in the main text.

Let´s consider a triple layer stack as sketched in Figure S1. The first and the last layer are semi-infinite media characterized by homogeneous and isotropic dielectric functions ε_1 and ε_3 respectively. The middle layer has a thickness d and an in-plane anisotropic dielectric function $\varepsilon_L = \varepsilon_2$. The transmission and reflection Fresnel coefficients for s-polarized incidence are:

$$t_{ij} = \frac{2C_i}{C_i + C_j}, \qquad (S1)$$

$$r_{ij} = \frac{C_i - C_j}{C_i + C_j}, \qquad (S2)$$

where $c_i = \sqrt{\varepsilon_i}\cos\theta_i$ and θ_i is the illumination angle. Taking multiple reflections into account (as sketched in Figure S1), the transmission coefficient for the three-layer system reads as[1, 2]

$$t_{123} = \frac{t_{12}t_{23}e^{i\beta}}{1 + r_{21}r_{23}e^{i2\beta}} \qquad (S3)$$

with $\beta = \frac{2\pi d}{\lambda}\sqrt{\varepsilon_2}\cos\theta_i$. Usually, the absolute transmission t_{123} is difficult to evaluate. However, the quantity t_{123}/t_{13} can be measured easily due to cancellation of common terms. We can also assume that system is illuminated at normal incidence with polarization along the eigendirection x of the anisotropic layer. The changes in transmission due to the presence of the thin layer can then be written as

$$\frac{\Delta t^x}{t_{13}} = \frac{t^x_{123} - t_{13}}{t_{13}} \qquad (S4)$$

Now, in the limit of small thickness $\ll \frac{\lambda}{2\pi\sqrt{\varepsilon_2}\cos\theta_i}$, the exponential factor can be expanded into $e^{i\beta} \sim 1 + \frac{2\pi d\, i}{\lambda}\sqrt{\varepsilon_2}\cos\theta_i$ and, for normal incidence illumination and using equation (S1), (S2) and (S3), equation (S4) can then be approximated to

$$\frac{\Delta t^x}{t_{13}} \sim \frac{2\pi d\, i}{\lambda} \frac{(\varepsilon_{L,x} - \sqrt{\varepsilon_1}\sqrt{\varepsilon_3})}{\sqrt{\varepsilon_1} + \sqrt{\varepsilon_3}}. \qquad (S5)$$

If the substrate is isotropic (as in this case), the analysis of the data is simplified as the rotation in transmission is small enough to be treated in the first order in the optical functions, similar to what was previously shown for reflection.[3] The rotation and ellipticity can then be written as

$$\theta + i\xi = \frac{t_{123}^x - t_{123}^y}{t_{123}^x + t_{123}^y} = \frac{\Delta t^x - \Delta t^y}{2\, t_{13} + (\Delta t^x + \Delta t^y)} \approx \frac{\Delta t^x - \Delta t^y}{2\, t_{13}}, \qquad (S6)$$

where we have assumed that the transmission without the presence of the layer is much larger than the changes in transmission due to the presence of the anisotropic metasurface, i.e. $2\, t_{13} \gg (\Delta t^x + \Delta t^y)$.

If measurements were performed in air ε_1=1, and combining equation (S5) and equation (S6), we obtain the result:

$$\theta + i\xi = \frac{\pi d\, i}{\lambda} \frac{(\varepsilon_{L,x} - \varepsilon_{L,y})}{1 + \sqrt{\varepsilon_3}} \qquad (S7).$$

If we introduce the refractive index of the substrate as $n_s = \sqrt{\varepsilon_3}$, we thus retrieve equation 1 discussed in the main text.

b. Transfer matrix approach

We presented in the main manuscript simulations of the metasurface using a transfer matrix formalism. In this approach, we model each dimer as two coupled prolate ellipsoids, apply Maxwell-Garnett effective medium approach to extract the layer dielectric function and finally apply the transfer matrix approach to retrieve the rotation. The polarizability tensor (in nm^3) of the single ellipsoid expression reads, in Gauss units, as follows[2]

$$\bar{\bar{\alpha}} = \frac{V}{4\pi}(\varepsilon - \varepsilon_m)\bar{\bar{I}} \cdot \left[\varepsilon_m \bar{\bar{I}} + (\varepsilon - \varepsilon_m)\left(\bar{\bar{L}} - \frac{k^2}{4\pi}\bar{\bar{D}} - ik^3\frac{V}{6\pi}\bar{\bar{I}}\right)\right]^{-1} \qquad (S8)$$

Where $V = 4\pi r_1 r_2 r_3/3$ is the volume of the ellipsoid with radii r_i ($i = 1,2,3$), $k = 2\pi n/\lambda$ the wavevector of the incoming light in the medium with index $n = \sqrt{\varepsilon_m} = \sqrt{({n_{sub}}^2 + {n_0}^2)/2}$ and ε is the dielectric function of gold.[4] We also took into account size effects such as retardation ($k^2\bar{\bar{D}}$) and radiative damping ($k^3 V\bar{\bar{I}}$).[5] Once the polarizability of the single ellipsoid composing the dimer is known we can proceed to evaluate the effective polarizability of the dimer. Using the coupled dipoles approximation and assuming the polarization plane of the incident electric field lying on the x-axis (direction defined by r_1 and also corresponding to the long-axis of the dimer), one can write the effective polarizability tensor as follows[6]

$$\overline{\overline{\alpha_{eff}}} = \begin{pmatrix} \alpha_{||} & 0 & 0 \\ 0 & \alpha_{\perp} & 0 \\ 0 & 0 & \alpha_{\perp} \end{pmatrix}, \qquad \text{(S9)}$$

with

$$\alpha_{||} = \frac{2\alpha_1 + 2{\alpha_1}^2 k^3 [A(kR) + B(kR)]}{1 - {\alpha_1}^2 k^6 [A(kR) + B(kR)]^2} \qquad \text{(S10)}$$

and

$$\alpha_{\perp} = \frac{2\alpha_1 + 2{\alpha_1}^2 k^3 A(kR)}{1 - {\alpha_1}^2 k^6 A(kR)^2} \qquad \text{(S10)}$$

Here, R is the distance between the centers of the two dimer building blocks, namely $2r_1 + g$, where g is the gap between the two disks. Experimentally g = 15 nm, which is also the value assumed in the calculations. The functions $A(kR)$ and $B(kR)$ read as:

$$A(kR) = \left(\frac{1}{kR} + \frac{i}{(kR)^2} - \frac{1}{(kR)^3}\right) e^{ikR} \qquad \text{(S11)}$$

$$B(kR) = \left(-\frac{1}{kR} - \frac{3i}{(kR)^2} + \frac{3}{(kR)^3}\right) e^{ikR} \qquad \text{(S12)}$$

Once the effective polarizability of the dimer is known, one can apply the Maxwell-Garnett Approximation for calculating the effective dielectric tensor of the metasurface layer made by the dimmers in contact with the glass substrate and the air. To do so we normalized the quantity expressed by Eq. (S9) to the volume of the dimer, namely $2V$, and obtained the following expression for the effective dielectric tensor[7]

$$\bar{\bar{\varepsilon}}_{eff} = \left(f_1 \bar{\bar{I}} + 2 f_2 \bar{\bar{\alpha}}_{eff}\right) \cdot \left(f_1 \bar{\bar{I}} - f_2 \bar{\bar{\alpha}}_{eff}\right)^{-1}. \qquad \text{(S13)}$$

In equation (S13) f_1 and f_2 are the filling factors of air and of the nanoparticles respectively. This quantity allow us to calculate the Fresnel transmission and reflection coefficients of a multilayered system, which is assumed to model the real system studied in the experiments.

To simulate the rotation, we first assume that the material is illuminated along the *x* direction and that the dielectric function of the material is rotated of $\phi = 45°$ with to its pricncipal axis. The dielectric function hence reads as[8]

$$\bar{\bar{\varepsilon}}_L = \begin{pmatrix} \bar{\bar{\varepsilon}}_{eff,x}\cos^2\varphi + \bar{\bar{\varepsilon}}_{eff,y}\sin^2\varphi & -\left(\bar{\bar{\varepsilon}}_{eff,x} - \bar{\bar{\varepsilon}}_{eff,y}\right)\cos\varphi\,\sin\varphi & 0 \\ -\left(\bar{\bar{\varepsilon}}_{eff,x} - \bar{\bar{\varepsilon}}_{eff,y}\right)\cos\varphi\,\sin\varphi & \bar{\bar{\varepsilon}}_{eff,x}\sin^2\varphi + \bar{\bar{\varepsilon}}_{eff,y}\cos^2\varphi & 0 \\ 0 & 0 & \bar{\bar{\varepsilon}}_{eff,z} \end{pmatrix} \quad \text{(S14)}$$

Using the Transfer Matrix Method,[9] it is now possible to calculate the complex transmission coefficients $t_{pp}, t_{ss}, t_{sp}\ t_{ps}$ .The rotation and ellipticity is then defined as

$$\theta + i\xi = \frac{t_{ps}}{t_{ss}} = \frac{t_{sp}}{t_{pp}} \quad \text{(S15)}$$

In the simulation, the dimensions of the single disk composing the dimer used to reproduce the experimental results are (diameter) D = 95 nm, (height) h = 45 nm, f_2 = 20%. The effective medium layer thickness was used as fitting parameter to reproduce the intensity of the measured quantities. In our case we assumed such a thickness to be 1.5h.

3) Additional results

a. Simulated extinction using FDTD

In Figure 2c we showed the near field intensity at λ = 650nm for the case of Au dimer in air supported on a glass substrate. For completeness, we show here in Figure S2 the extinction for the same dimer structure using a filling factor of 12%. A precise agreement can be expected if one considers broadening caused by the morphological dispersion within the sample.

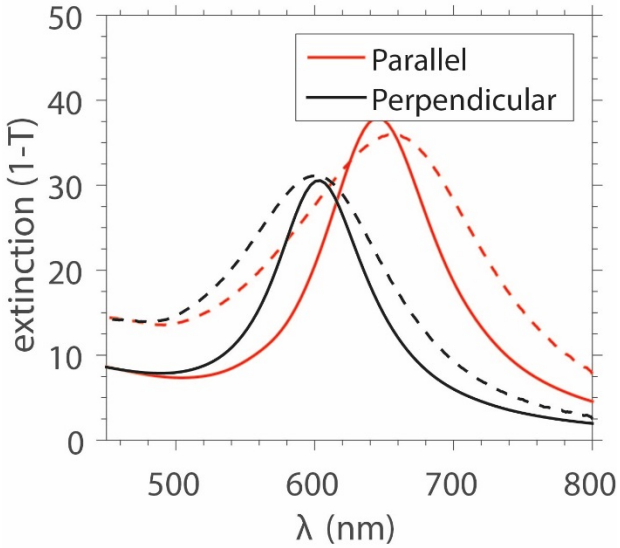

Figure S2. Extinction of Au dimer calculated by FDTD (full lines) and measured (dashed line, also shown in Figure 1b) for polarization parallel and perpendicular to the dimer axis.

b. Tunability of the rotation angle

In Figure 2 in the main text we plot the rotation for a dimer and we relate the response to the optical anisotropies of the metamaterial. When two in-plane modes are measured the rotation is in fact related to the difference in the in-plane polarization dependent extinction spectra. This offers a very intuitive method to tune the rotation: by engineering the geometrical parameters of the nanoparticles constituting the metasurface, changes in the rotation peak can be achieved. This is shown in Figure S3a and S3b, where the calculated ellipticity and rotation are shown for different single particle aspect ratios, and keeping the other parameters (gap, filling factor, dielectric function of the medium,…) unmodified. The calculations were performed using the transfer matrix method presented in the previous section. The aspect ratio is defined as the ratio between the in-plane axis along the dimer direction and the axis perpendicular to it. AR =1 thus corresponds to a dimer where each disk is symmetric. In particular, in these simulations, the in-plane axis perpendicular to the dimer axis and the height of the nanoparticles were kept constant to 95 nm and 45 nm respectively and the in-plane axis along the dimer direction was progressively increased.

In Figure S3c and S3d we also show that it is possible to increase the rotation at a fixed wavelength by playing with the size of the particles in the dimer. Size 1 corresponds to an ellipsoid with semiaxis of r_1 = 47.5 nm, r_2 = 47.5 nm and r_3= 22.5 nm. Size 2 (AR 1.5) corresponds to an ellipsoid with semiaxis of r_1 = 48.75 nm, r_2 = 32.5 nm and r_3= 22.5 nm and Size 3 (AR 2) corresponds to an ellipsoid with semiaxis of r_1= 50 nm, r_2= 25 nm and r_3= 30 nm. All these simulations were performed in air, using the same filling factor and embedding medium as in Figure 2f in the main text.

In Figure S4 we also experimentally verified the possibility of tuning the peak by changing the in-plane diameter and keeping the other parameters constant. This was realized following the same HCL recipe described in the methods section. The only differences were the size D_{PS} of the polystyrene beads (from 60 nm to 120 nm) and the deposition angle Θ which was tuned, depending on the diameter of the polystyrene beads, from 11.5° to 16.3°, according to the formula:

$$\Theta = \mathrm{atan}\left(\frac{g+D_{PS}}{2\,(T_{PMMA}+T_{MASK})}\right)$$

where T_{PMMA} is the thickness of the PMMA layer spinned and T_{MASK} is the thickness of the deposited metal mask. The resonances are shifted to the shorter wavelength when compared to the rotation shown in Figure 2 simply because in this case no adhesion layer was used. One can notice in Figure S4b a clear shift in the rotation resonance for increasing diameter of the nanoparticles, similar to the extinction resonance measured in the same samples (Figure S4a).

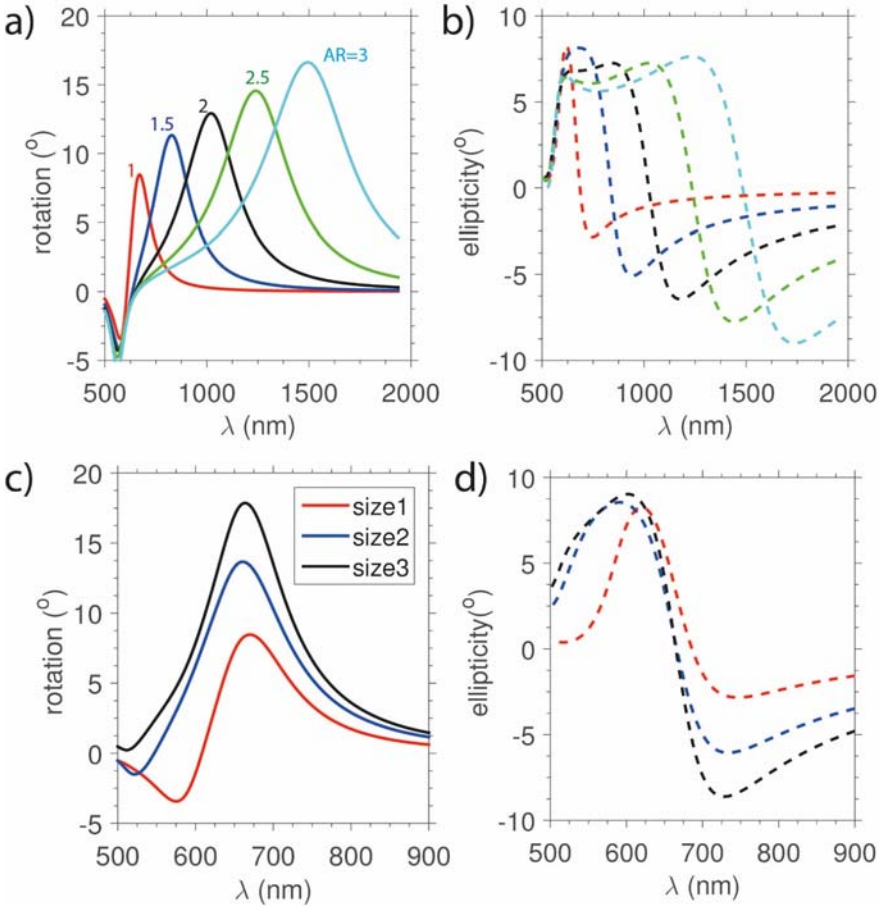

Figure S3. Tunability of the simulated rotation. Calculated rotation(a) and ellipticity (b) for metasurfaces of Au dimers for different in-plane aspect ratio (AR): larger rotations and shifts in the rotation peaks are observed for increasing aspect ratios due to further detuning of the in-plane resonances. (c) rotation and (d) ellipticity for various nanoparticle sizes. The rotation at a specific wavelength can be increased by appropriate choices of the dimer dimensions.

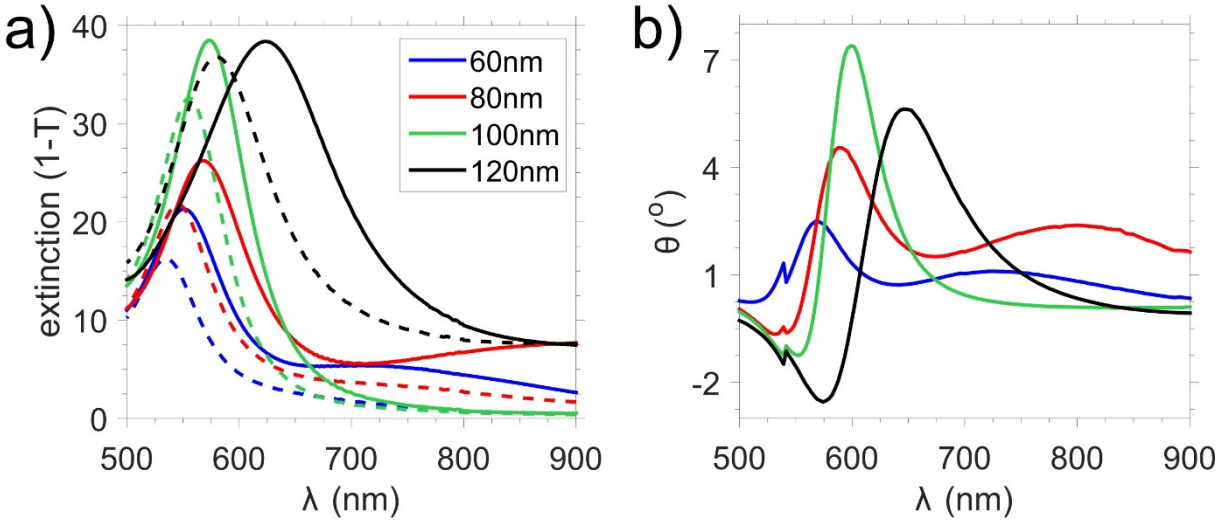

Figure S4. Peak tunability of the polarization rotation. (a) Experimentally measured extinction for polarization parallel (full lines) and perpendicular (dashed lines) to the dimer axis in anistropic metasurfaces composed of gold dimers with different diameters as indicated in the legend. To fabricate the nanostructures the deposition angle was modified to keep the gap constant to ~15nm.

(b) Rotation for the same metasurfaces. The positive peak in the rotation can be changed in the visible region simply by tuning the geometrical parameters.

c. Bulk refractometric sensing

In Figure 3 in the main text, we show the measured changes in rotation when the dielectric function of the medium was changed from water to a mixture of water and ethylene glycol. For completeness, we plot in Figure S5 the measured rotation as a function of wavelength.

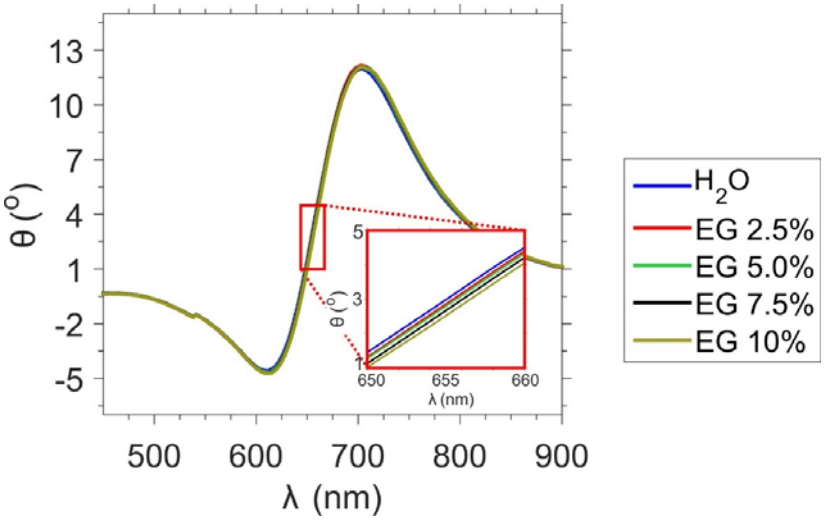

Figure S5. Bulk refractive index using polarization rotation. Spectra in different refractive index liquids. In the inset one can observe red shift in the resonances for increasing ethylene glycol concentration.

d. Relation between rotation and refractive index sensitivity

In the main text it is argued that an optimization of the metamaterial properties can result in an increase in the detection sensitivity. In Figure S4 we also showed that by changing the size of the particles within a dimer, one can increase the rotation at a fixed wavelength. However, it is not readily clear that an increase in the rotation corresponds in an increase in the rotation sensitivity during changes in the refractive index of the medium surrounding the particles. Using the transfer matrix approach, we verified that this is exactly the case in Figure S6. Figure S6a shows the rotation spectra in water for the 3 different nanoparticle sizes shown in Figure S3c. Afterwards, we changed the dielectric function of the medium surrounding the particles from 1.33 (water) to 1.35 and calculated the changes in rotation as a function of wavelength. The results are shown in Figure S6b: we verified that a larger increase in the rotation $\Delta\theta$ per refractive index unit can effectively be realized.

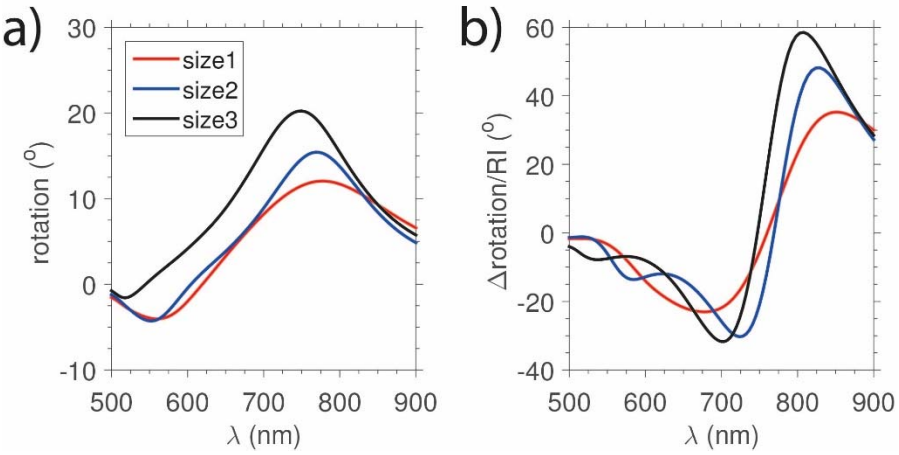

Figure S6 (a) Calculated rotation for nanoparticles of different sizes in water. (b) Calculated changes in rotation per refractive index unit for the three different sizes. The rotation sensitivity can thus be increased by augmenting the rotation of the metasurfaces.

d. Alternative set up for measuring the rotation angle

We present in Figure S7 an alternative sensing set up based on a double detector system. This experiment has a twofold scope: first, it illustrates clearly how to relate the changes in transmission during molecular adsorption to rotation, and second it demonstrates that rotation can be measured without the need of a PEM and a lock-in.

In brief, after transmission a beam splitter was inserted and the light for polarization parallel and perpendicular to the dimer axis can be measured using a spectrometer. Similar to standard LSPR sensing each peak is tracked during molecular adsorption for both polarizations along and perpendicular to the dimer axis. We show this in Figure S7b, for the two resonances. As expected, one can notice a much larger change for polarization parallel to the dimer axis rather than in the perpendicular direction. From the transmission T, the rotation in degrees can be calculated as $\theta = \frac{180(T_x - T_y)}{\pi(T_x + T_y)}$. If one would also use single wavelength illumination and photodiode, the setup can be turned into a spectrometer-free system. This configuration was recently demonstrated to be also stable to drift during catalytic sensing measurements.[10]

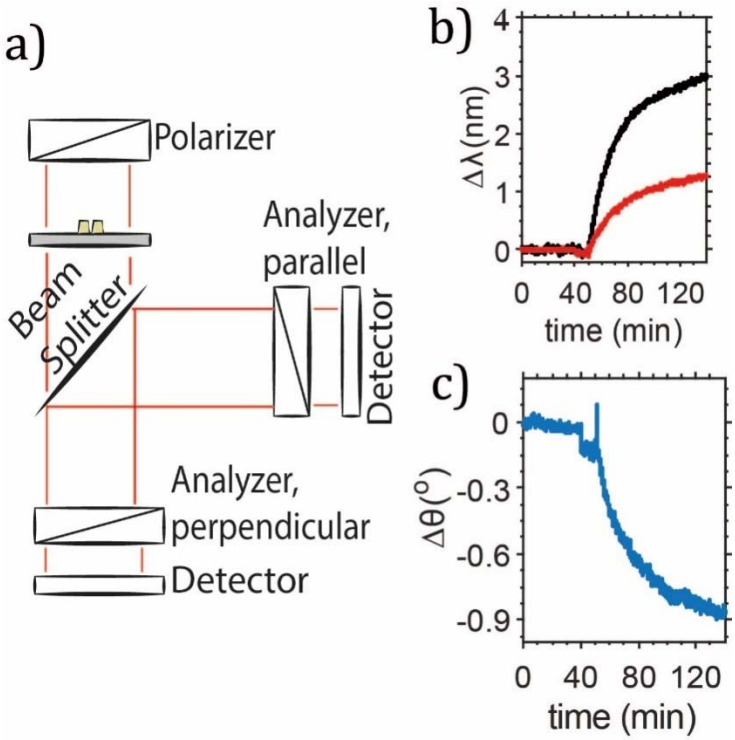

Figure S7. (a) Sketch of the double detector setup utilized in this experiment. (b) In this case, it was possible to perform standard refractometric sensing as the detector consisted of two spectrometers. The two peaks corresponding to the parallel and perpendicular in-plane modes of the dimers were tracked during NA adsorption (black and red line respectively). One can notice the larger sensitivity of the parallel mode. (c) Measured rotation using a double analyzer/detector setup in the region of maximum sensitivity.

1. Born, M.; Wolf, E., *Principles of Optics (4th.ed.)* Pergamon Press, **1970**.
2. Bohren, C. F.; Huffman, D. R., *Absorption and Scattering of Light by Small Particles,* Wiley, **1983**.
3. Aspnes, D. E.; Studna, A. A. *Phys. Rev. Lett.* **1985,** 54, (17), 1956-1959.
4. Johnson, P. B.; Christy, R. W. *Physical Review B* **1972,** 6, (12), 4370-4379.
5. Meier, M.; Liao, P. F.; Wokaun, A. *J. Opt. Soc. Am. B* **1985,** 2, (6), 931-949.
6. Boris, K.; Andrei, M.; Vladimir, Z.; Nikolai, K. *Nanotechnology* **2006,** 17, (5), 1437.
7. Choy, T. C., *Effective Medium Theory* Oxford University Press: 1999.
8. Ogier, R.; Fang, Y.; Käll, M.; Svedendahl, M. *Phys. Rev. X* **2015,** 5, 041019.
9. Schubert, M. *Physical Review B* **1996,** 53, (8), 4265-4274.
10. Wadell, C.; Langhammer, C. *Nanoscale* **2015,** 7, (25), 10963-10969.